The surface boundary conditions for quantum evaporation in ^{4}He

1990 J. Phys.: Condens. Matter 2 5025

(http://iopscience.iop.org/0953-8984/2/22/022)

J. Phys.: Condens. Matter 2 (1990) 5025–5046. Printed in the UK

The surface boundary conditions for quantum evaporation in ^{4}He

M Brown and A F G Wyatt
Department of Physics, University of Exeter, Stocker Road, Exeter EX4 4QL, UK

Received 23 November 1989

Abstract. Quantum evaporation of ^{4}He atoms by phonons and rotons in liquid ^{4}He is measured for a wide range of conditions. The results confirm that an atom is evaporated in a single-excitation→single-atom process and that the boundary conditions of conservation of energy and parallel momentum are obeyed. Excitations in the liquid are generated by pulse heating a thin metal film heater, and the evaporated atoms are detected by the energy yielded on condensation at the surface of a superconducting transition edge bolometer. The heater and bolometer can be rotated about a common axis in the liquid surface, and the collimation of the excitations and atoms into beams allows the angles of incidence and evaporation to be defined. It is first shown that the input power and pulse length must be carefully chosen to produce beams of phonons and rotons that are fully ballistic. The time of flight from the heater to the bolometer is measured, and the angular distribution of the evaporated atoms is determined for different angles of incidence. In particular, the wavevector dependence of the roton→atom pulse shape can be seen. We see no sign of Pitaevskii roton decay over the long liquid path lengths involved ($\sim$ 6 mm), and there is no indication that ripplons are created in the evaporation process.

1. Introduction

In this paper we investigate the single-excitation→single-atom quantum evaporation process for the desorption of atoms at the free surface of liquid ^{4}He by phonons and large wavevector rotons. Measurements of the time of flight of the atom signals produced by a short heat pulse in the liquid, together with the angular distribution of the evaporated atoms, show that at the boundary both the energy and the component of momentum parallel to the surface are conserved [1–3]. The results presented here extend these earlier measurements and compare them to model calculations. One conclusion is that surface excitations (ripplons) are not involved to a significant extent. The existence of the quantum evaporation process makes it possible to investigate the way that high-energy excitations are generated by thermal sources in liquid helium, and the manner in which they propagate over macroscopic distances in the bulk liquid. For example, the power and duration of the input heat pulse are found to be very important in determining whether or not the injected excitations will subsequently propagate ballistically over the distances of several millimetres typically used in experiments. Hence, the input conditions required to produce either phonons or rotons are very different. However, these aspects of the injection of excitations into the bulk liquid will be considered in detail in another paper, and here we mainly consider the evaporation mechanism itself.

0953-8984/90/225025+22$03.50

In addition to the intrinsic interest of the quantum processes at the free surface of the liquid, an understanding of the evaporation mechanism opens up the possibility of giving a complete microscopic description of the dynamic balance between liquid helium and its saturated vapour at low temperatures. The first measurements directly related to this problem [4] showed that the vapour immediately above the surface of liquid helium only exchanges energy with the normal fluid, namely the bulk excitations. It was then suggested [5] that the evaporation of atoms is dominated by single-excitation→single-atom processes. Note that for liquid helium in thermal equilibrium the flux of excitations incident on the liquid surface does not have a singularity at the roton minimum because the divergence in the energy density of states at this point is exactly compensated for by the vanishing group velocity [6], but it is now clear that rotons with negative group velocity can quantum evaporate [7]. This led to the idea that the saturated vapour pressure can be determined by the balance of evaporation and condensation processes of this type [8].

The earliest attempt to observe the quantum evaporation of atoms used a time-of-flight technique, with excitation path lengths in the liquid of several millimetres [9]. Although fast evaporation signals were detected the results could not be interpreted in terms of the desorption of one atom by a single excitation. The first unambiguous measurement of the quantum evaporation of atoms by phonons used a similar time-of-flight technique [1], and also showed that desorption of surface bound ^{3}He atoms is possible. The separate evaporation of atoms by phonons and large wavevector rotons (those with wavevectors greater than that at the roton minimum, $q_{\min} = 1.92\,\text{Å}^{-1}$) was subsequently observed by measuring the angular distribution of the evaporated atoms [2]. The results were found to be generally consistent with the boundary conditions described above.

The main aim of the work presented here is to extend the earlier evaporation measurements over a much wider range of input powers and angles. Now that the conditions required for producing ballistic excitation beams are better understood it is possible to make detailed comparisons between the measured results and those from a model calculation.

There is at present no satisfactory theoretical description of the evaporation process. Early calculations [10], which used a weak tunnelling Hamiltonian for the interaction at the surface, gave results that are inconsistent with more recent experimental measurements. In particular, such a theory predicts a large value for the reflection coefficient for atoms incident on the free surface from the vacuum, whereas the measured reflection coefficient for both elastic and inelastic processes is very small ($\lesssim 1\%$ [11]). The equilibrium saturated vapour pressure of liquid ^{4}He at low temperatures can be accounted for by a dynamic balance of quantum evaporation and corresponding quantum condensation processes if the *average* quantum efficiency of allowed processes is 1/3 [8]. To explain the damping of shear waves by roton quantum evaporation a value of around 1/3 was found to be necessary [12].

2. Quantum evaporation

The quantum evaporation of an atom, shown in figure 1(*a*), is assumed to obey the following relations for energy and momentum conservation:

$$\frac{\hbar^2 k^2}{2m_4} = \hbar\omega - E_b \tag{1}$$

and

$$\hbar q \sin\theta = \hbar k \sin\phi \tag{2}$$

where $\hbar\omega$ and $\hbar q$ are the energy and momentum of the excitation, $\hbar k$ is the momentum of the evaporated atom and m_4 is the mass of a free ^{4}He atom. The angles θ and ϕ are the angles of incidence and evaporation as defined in figure 1(a). The energy $E_b = 7.16$ K is the binding energy of a ^{4}He atom to the bulk liquid [13] and is the minimum energy an excitation must have in order to desorb an atom at the surface. Conservation of momentum in the plane of the free surface follows from the presumed translational invariance of the interface between the liquid helium and the vacuum. The detailed consequences of these two conditions are considered in [8], and only the main features are discussed here.

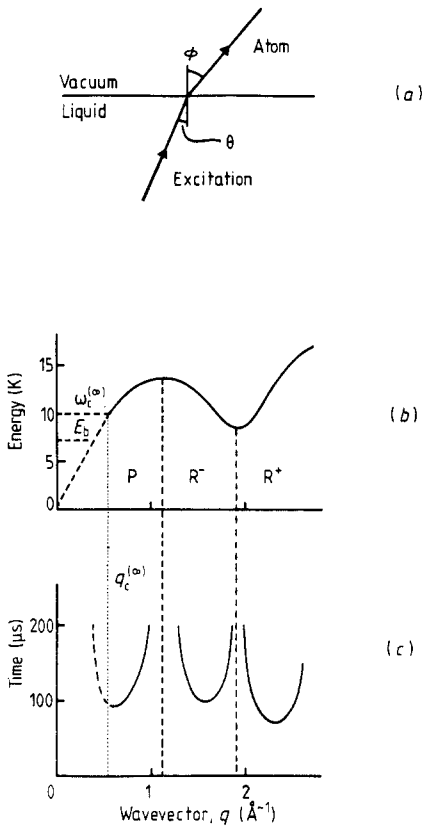

Figure 1. (a) A schematic representation of the quantum evaporation process at the free surface of liquid ^{4}He which defines the angles θ and ϕ. (b) The dispersion curve for excitations in liquid ^{4}He at SVP [25]. (c) The calculated time of flight for an excitation→atom process for the path lengths used in the present experiment (figure 3) shown as a function of the wavevector of the excitation.

It is convenient to divide the excitation spectrum into three sections (figure 1(b)). The first of these is the phonon section (P), which includes all excitations up to the maxon point at $q \simeq 1.1$ Å^{-1}. The anomalous dispersion of phonons in liquid helium, i.e. the phase velocity of the excitations initially increases with wavevector, means that

phonons below certain critical cut-off wavevectors are unstable against spontaneous decay [14]. These cut-off wavevectors are usually denoted by $q_c^{(n)}$ to indicate the decay of one high-energy phonon into n smaller phonons. Their values are obtained from neutron scattering determinations of $\omega(q)$ [15], and lie in the range $q_c^{(2)} = 0.46\,\text{Å}^{-1}$ to $q_c^{(\infty)} = 0.55\,\text{Å}^{-1}$. The phonon mean-free-path has not been measured, but calculations indicate that it becomes very short, less than $\sim 1000\,$Å, as the wavevector increases to the cut-off at $q_c^{(2)}$ [16, 17]. The mean-free-paths associated with each order of spontaneous decay are not known, but they are likely to be shorter than the path length in the liquid helium used in the experiments described here ($\sim 6.5\,$mm). Since the excitations are stable for $q > q_c^{(\infty)} = 0.55\,\text{Å}^{-1}$, it is this value that is taken as the threshold for propagation over macroscopic distances. The cut-off at $q_c^{(\infty)}$ corresponds to a phonon energy of $\hbar\omega_c^{(\infty)} = 10.0\,\text{K}$ [15]. This value is close to the measured cut-off energy for phonon propagation of $9.5 \pm 0.4\,\text{K}$ [18], which was determined for slightly shorter propagation distances ($\leq 2.5\,$mm) in the liquid.

The roton curve is separated into two sections, one on either side of the roton minimum at $q_{\min} = 1.92\,\text{Å}^{-1}$. Rotons with $q < q_{\min}$ have group velocities which are oppositely directed to their momenta, and will be referred to as 'R$^-$ rotons'. Those rotons with wavevectors greater than $q_{\min}$ have their group velocities and momenta parallel to one another and are correspondingly referred to as 'R$^+$ rotons'. The long mean-free-paths found for rotons shows that they are stable against spontaneous decay.

It has been suggested that the spontaneous emission of small phonons by rotons in the region $q \sim 2.2$–$2.4\,\text{Å}^{-1}$ can occur if the roton group velocity exceeds the ultrasonic phonon velocity c_0 [19]. However, the excitation group velocities calculated from neutron scattering measurements of $\omega(q)$ are not sufficiently accurate to determine whether c_0 is exceeded or not. The existence of such a decay mechanism should produce an increase in the measured neutron scattering linewidths of these rotons—an effect known as Pitaevskii broadening. These linewidths have only been determined with high resolution for liquid ^{4}He at an ambient temperature of 1 K, and they are found to be no greater than the thermally induced excitation linewidths at this temperature [20]. These measurements can therefore only be used to place a *lower* limit of $\sim 10^{-10}\,$s on the roton lifetime at temperatures below $\sim 1\,$K. The corresponding estimate of the minimum mean-free-path is $\lambda \simeq c_0 \Delta t \simeq 1000\,$Å. This minimum value of λ for the spontaneous emission of a phonon is still very short compared with the propagation distances of several millimetres required in evaporation experiments. Quantum evaporation measurements therefore provide an alternative method for examining the lifetime of these excitations. If the R$^+$ rotons in this part of the dispersion curve are indeed stable then all the excitations indicated by the full curve in figure 1(*b*) should contribute to the flux reaching the free surface. R$^+$ rotons with energies greater than $14.32\,\text{K}\,(= 2E_b)$ can in principle evaporate two atoms.

For excitation and atom path lengths l_e and l_a respectively, the total flight time for a ballistic evaporation process is given by

$$t = \frac{l_e}{v_e(q)} + \frac{l_a}{v_a(k)} \tag{3}$$

where $v_e(q)$ is the excitation group velocity in the liquid, and $v_a(k)$ is the atom group velocity. Using equation (1) and the measured dispersion curve $\omega(q)$, the total time t can be calculated entirely in terms of the excitation wavevector q, as shown in figure 1(*c*). These values of t are calculated for the actual path lengths used in the

experiment ($l_e \simeq l_a \simeq 6.5$ mm—see section 3). The combined effect of the different dispersion of excitations and free atoms gives rise to characteristic minimum signal times for evaporation from each section of $\omega(q)$. Since these minimum times are different for evaporation by phonons, R^-, and R^+ rotons, total time-of-flight measurements can be used to discriminate between the three sections of the excitation spectrum. This was the basis of the first quantum evaporation experiment [1].

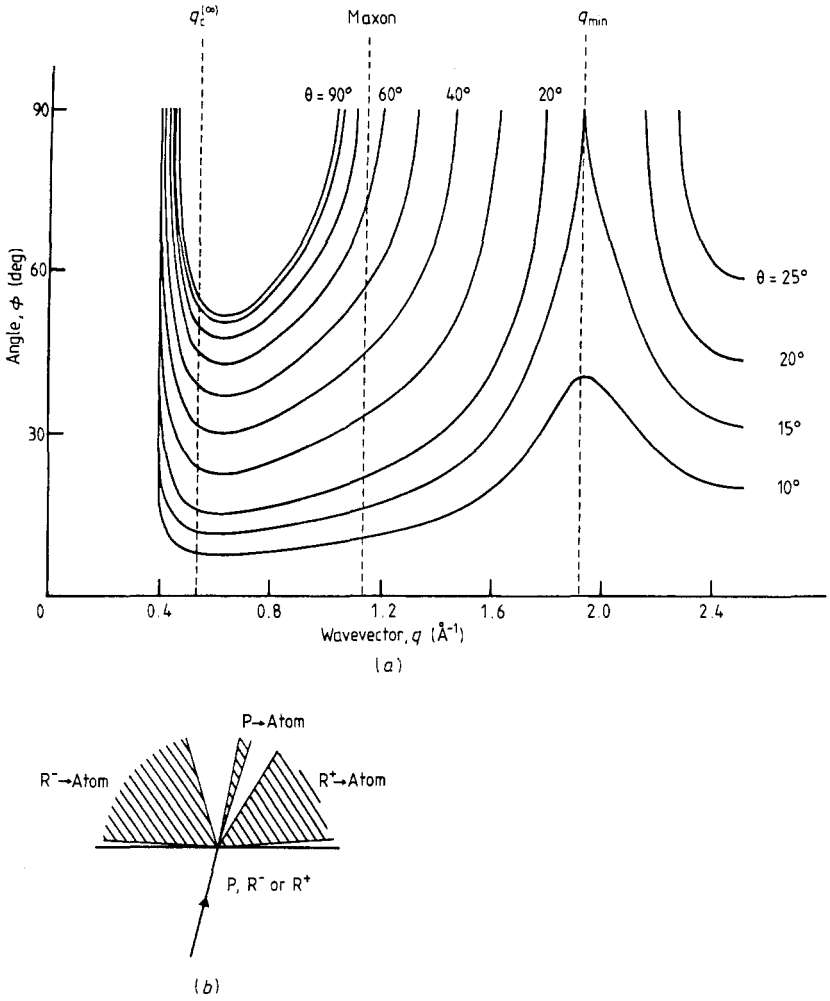

Figure 2. (*a*) The angle of evaporation ϕ (figure 1(*a*)) as a function of the excitation wavevector q for different angles of incidence θ (after [8]). (*b*) The angular separation of atoms evaporated by phonons (P), R^- rotons, and R^+ rotons for the angle of incidence $\theta = 14°$.

The evaporation of atoms by different excitations can also be separated using the 'refraction' effect at the surface implied by equation (2). This effect is summarised in the diagram in figure 2(*a*), in which the evaporation angle ϕ is shown as a function of the excitation wavevector for a series of different angles of incidence θ [8]. Generally, roton→atom processes produce a larger change in direction at the surface than phonon→atom processes, since rotons have much more momentum. Phonons with

$\hbar\omega \simeq E_b$ would be an exception to this, but as these phonons have wavevectors well below $q_c^{(\infty)}$ they have very short mean-free-paths and decay before reaching the free surface. The resulting angular separation of different evaporation processes is shown schematically in figure 2(*b*). This diagram also illustrates the unusual 'back refraction' effect expected for R^- roton→atom processes, which arises because the wavevectors of these rotons are oppositely directed to their group velocities.

3. Experimental

Figure 3 shows the main elements of the experimental apparatus. The source and detector assemblies are mounted on two independent wheels, each driven via a short gear train by a miniature superconducting stepping motor. The heater H consists of a 1 mm square gold film, ~ 70 Å thick, evaporated onto a glass substrate. This has a resistance at 4.2 K of ~ 60Ω. The heater is surrounded by the shrouding S1, made from a sheet of sintered copper, which prevents unwanted excitations reaching the liquid surface, and reduces the number reflected back into the direction of the main forward flux. The collimator C1 is made from sheet mica, ~ 50 μm thick, in which a 0.4 mm × 1.0 mm slot is punched, with the smallest dimension in the plane of the figure. The dimensions chosen are necessarily a compromise between angular resolution and signal size.

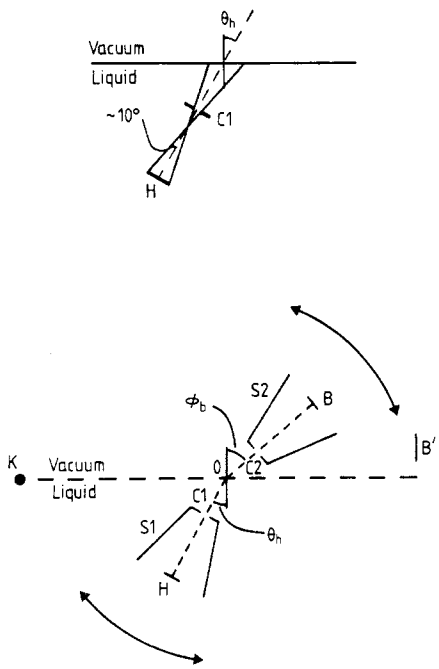

Figure 3. Schematic diagram of the experimental arrangement (see text). The upper diagram shows the range of angular directions defined by the heater and collimator dimensions, in the plane of rotation of the experiment. Dimensions: O–H, 6.55 ± 0.15 mm; O–B, 6.55 ± 0.15 mm; O–C1, 2.50 ± 0.10 mm; O–C2, 2.45 ± 0.15 mm.

A similar arrangement provides collimation and screening for the bolometer B, except that in this case the shrouding S2 is made from mica sheeting. The bolometer itself consists of a 1 mm square zinc film, evaporated onto a glass substrate. The film is scratched to produce a serpentine track giving a low-temperature normal resistance of $\sim 70\,\Omega$. The bolometer is then operated as a constant temperature detector, held at fixed point on its transition curve by a static magnetic field and a bias current provided by a fast feedback circuit [21].

The angles θ_h and ϕ_b in the figure define the positions of the heater and bolometer. These are measured potentiometrically using two resistance windings, taken from commercial $0-10\,k\Omega$ ten-turn potentiometers, one mounted behind each main wheel. This system gives a working range of $\sim 300°$ and a resolution of $\sim 1°$, with a maximum systematic calibration error of $\sim 3°$. Sliding contact to the windings is made using gold plated phosphor bronze wiper arms. The range of angles defined by the collimation is $\sim \pm 10°$ on each side of the directions θ_h and ϕ_b (see upper diagram in figure 3).

The correct depth of liquid is set using a heater K made from thin Karma resistance wire (from British Driver Harris), placed at the required height in the cell and level with the axis of rotation of the wheels. While in the vapour this heater produces an evaporation signal that can be detected by the additional bolometer B′. This signal falls by several orders of magnitude as soon as the liquid reaches the wire, with nearly all of the input energy then being dissipated directly into the bulk superfluid. Use of pure helium is particularly important in these experiments because at low temperatures impurity ^3He atoms go to the free surface, and can thus contribute to the evaporation signals [1]. Isotopically pure ^4He is therefore used throughout†, with a measured residual ^3He content of 6 ± 4 parts in 10^{10}‡.

The apparatus is cooled down to an operating temperature of $(100 \pm 10\,mK)$ using a $^3He/^4He$ dilution refrigerator. The ambient temperature of the experiment is monitored with a carbon resistance thermometer thermally anchored to the mixing chamber. The main evaporation measurements are made by pulsing the main heater H and recording the thermal response of the bolometer B to the resulting flux of evaporated atoms. The data is captured using a Biomation 8100 transient recorder and a purpose built signal averager, which can process data sets of 1024 points at ~ 250 per second. Typical evaporation signals require between 10^4 and 10^5 averaged repetitions to achieve acceptable signal-to-noise ratios.

The angular alignment and calibration of the system is determined optically at room temperature using an LED mounted behind the heater and a photodiode mounted behind the bolometer. An angular response function is then measured for a number of positions of the main wheels to check that the rotation is about the correct axis. An angular measurement is also made at $\sim 100\,mK$ using helium atoms evaporated directly from the superfluid film covering the heater. The liquid level in the cell is well below the heater and bolometer for this measurement. This provides a check that the collimation is fully effective for ^4He atoms at low temperatures, and that the propagation in the vapour is indeed ballistic for the typical fluxes involved in the evaporation experiments.

† Isotopically pure ^4He was obtained from P V E McClintock, University of Lancaster, UK.

‡ The residual ^3He content was measured by the US Bureau of Mines (Department of the Interior), Amarillo, Texas, USA.

4. The generation of ballistic excitations

It is now known that the heater input pulses must have a very low total energy for the evaporation of atoms by ballistic excitations to be observed [22]. Large energy inputs generate a high density of excitations in the helium, producing many interactions in the region in front of the source, and possibly some scattering within the beam as it propagates towards the surface. Such processes will affect the energy distribution of the excitations and reduce the effectiveness of the collimation. Low ambient temperatures are required to minimise the effects of interactions with bulk thermal excitations. However, some compromise is usually required between the ambient temperature and the input repetition rate so that acceptable signal-to-noise ratios can be achieved in the averaged data. In order to observe the evaporation of atoms by phonons, temperatures of less than $\sim 200\,\mathrm{mK}$ are required, and it seems likely that even at $\sim 100\,\mathrm{mK}$, the temperature used in the present evaporation experiments, interactions with thermal phonons via the 4-phonon–phonon process still have some small effect [23].

Although the input pulses used in previous experiments [1,2] were of sufficiently low energy for quantum evaporation by ballistic phonons and R^+ rotons to be identified, we have found that the details of the evaporation mechanism can only be seen clearly using considerably smaller energy inputs. It turns out that the conditions required to see evaporation by ballistic phonons are quite different from those needed for R^+ rotons. Examples of results obtained using different input conditions are shown in figures 4(*a*) and (*b*). All the input powers referred to in this paper are given in terms of the attenuation in decibels of a pulse of power 0.5 W applied to the $1\,\mathrm{mm}^2$ area of the heater. The atom signals are recorded for two different combinations of the heater and bolometer positions, which are selected to show respectively only phonon→atom or R^+ roton→atom evaporation.

Using the arrangement shown in figure 4(*a*) very short input pulses are found to produce fast narrow atom signals that can be readily identified with quantum evaporation by high-energy phonons. For values of the input pulse length t_p around $0.5\,\mu\mathrm{s}$ (the exact value depends on the heater power), this fast signal saturates and shows no further increase in amplitude, however long the input pulse is made. This effect is very clear from the measured traces given in figure 4(*a*), which show that there is almost no increase in the amplitude of the fast part of the signal even when the pulse energy is increased by a factor of 50 by increasing the pulse length from $t_p = 0.2\,\mu\mathrm{s}$ to $t_p = 10\,\mu\mathrm{s}$. It seems likely that this saturation of the signal is due to the scattering of the high-energy phonons by the injected low-energy phonons. A similar effect is also observed as the pulse power is increased, but there is not such a rapid dependence on the total energy input as when the pulse length is varied. For much longer pulses, with $t_p \gtrsim 5\,\mu\mathrm{s}$, a large slow signal develops after the ballistic phonon→atom signal. This component is identified with the evaporation of atoms by R^+ rotons that are scattered within the excitation beam during propagation to the surface, and that can therefore be seen at a 'phonon→atom' detector position. Previously [24], this feature was ascribed to 'diffusive' phonons, but the angular dependence measured at high powers now indicates that it is due to R^+ rotons.

In contrast to the behaviour of phonons, it is mainly the input pulse power that has an effect on the evaporation signals produced by R^+ rotons, as shown in figure 4(*b*). We find that only for powers less than $\sim -21\,\mathrm{dB}$ (4 mW) are the measured signals fully consistent with evaporation by ballistic R^+ rotons. The received pulse shapes can then largely be explained by assuming a simple thermal spectrum of rotons with flight

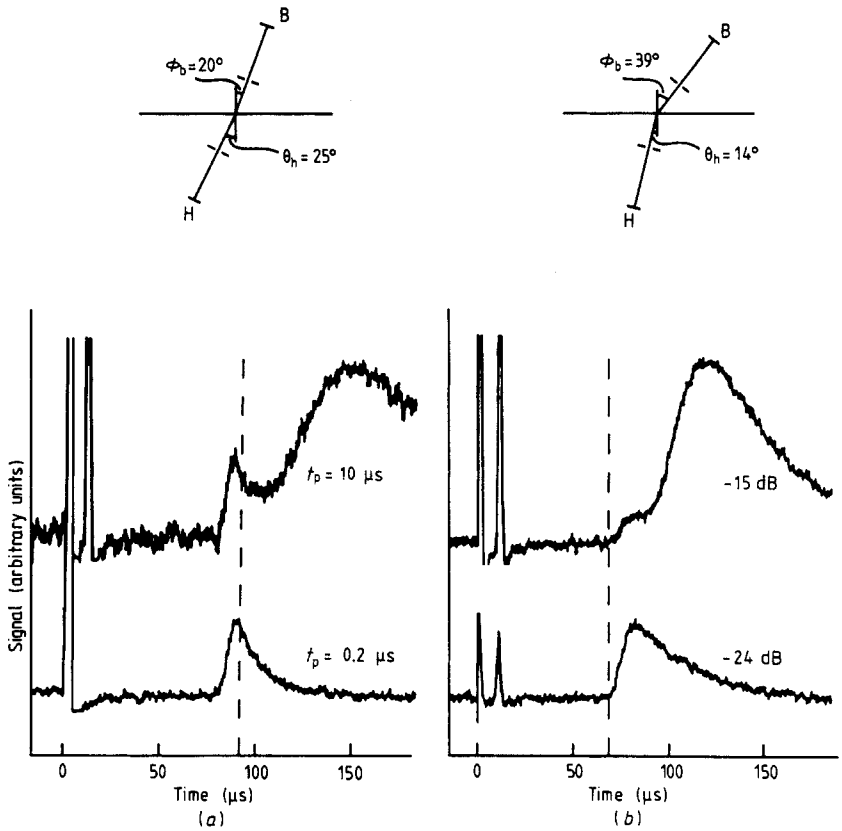

Figure 4. (*a*) Atom signals detected using a phonon→atom arrangement of the experiment for two different input pulse lengths, $t_p = 10\,\mu s$ (upper curve) and $t_p = 0.2\,\mu s$ (lower curve). The input power is −12 dB (31.5 mW). The broken line shows the calculated minimum time for the phonon→atom process. (*b*) Atom signals detected using an R^+ roton→atom arrangement for two different input powers, −15 dB (upper curve) and −24 dB (lower curve). The input pulse length is 10 μs. The broken line shows the calculated R^+ roton→atom minimum signal time.

times calculated for entirely ballistic propagation in the liquid. For these low heater powers the amplitude of the R^+ roton→atom signal is approximately proportional to the pulse length, and so longer pulses can be used to obtain reasonable signal-to-noise ratios. Nevertheless, for $t_p \lesssim 5\,\mu s$ the details of the pulse shape do depend on the length of the input pulse. The slower broad feature that dominates the pulse shapes for powers greater than ~ −18 dB (8 mW) is again thought to be due to rotons that have undergone some scattering by other injected excitations before reaching the surface.

The broken lines in figures 4(*a*) and (*b*) indicate the predicted minimum signal times for quantum evaporation by ballistic phonons and R^+ rotons respectively. These calculations use the results of neutron scattering measurements to obtain the excitation energies $\hbar\omega(q)$ and the group velocities $v_g(q)$. The agreement between the measured and calculated minimum time for evaporation by R^+ rotons provides strong evidence for the ballistic propagation of fast rotons. This also confirms that the conservation of energy at the surface is described by equation (1), since this condition determines the atom velocity. The phonon→atom results, however, show a signal arriving somewhat

earlier than is predicted with this model. This discrepancy is quite noticeable in the present results, and is $\sim$ 10% of the total flight time. On re-examination of previous experiments it appears that some discrepancy is always present, although to a lesser extent. Despite some variation in the exact value of this timing difference, the measured signals are typically 5% faster than is calculated. This is discussed later in section 5.5.

The estimated amplitude of the low-energy evaporation signals (the lower traces in figures 4(*a*) and (*b*)) is $\sim$ 1 nW. The total energy detected in the whole signal, integrated over $\sim$ 100 μs from the start of the signal, is therefore $\sim 5 \times 10^{-14}$ J. Assuming 100% detection efficiency of the energy of the atoms, this value corresponds to the detection of $\sim 3 \times 10^8$ evaporated atoms. The signal-to-noise ratio is $\sim$ 30 for 64k repetitions. However, the absolute flux of excitations produced by the heater has not yet been determined, so we cannot obtain the quantum efficiency of the evaporation process.

To summarise, the type of input pulses required for the observation of evaporation by ballistic phonons and R^+ rotons are found to be quite different. The generation of long mean-free-path high-energy phonons requires very short high-power pulses, unlike the much lower-power long pulses needed to see R^+ roton$\rightarrow$atom evaporation. In the earlier angular experiment [2], in which a 10 μs/$-$17 dB (10 mW) pulse was used, most of the input pulse length would have been ineffective in injecting ballistic phonons that could propagate freely to the surface. The phonon$\rightarrow$atom signals therefore appear very small relative to the heater power, due to the saturation effect described above. Also, an input power of -17 dB is too high to see fully ballistic propagation of R^+ rotons. With a better understanding of this system some of the details of the quantum evaporation process can now be examined.

5. Results

5.1. The evaporation of atoms by phonons

The angular dependence of the phonon$\rightarrow$atom evaporation signals is measured using a heater position $\theta_h = 25°$, and an input pulse of 0.05 μs at -14 dB (20 mW), as shown in figure 5(*a*). The signals only occur over a small range of detector angles, $15° \lesssim \phi_b \lesssim 35°$, and the amplitude varies smoothly as the detector is moved round. Since the velocity dispersion of the dominant phonons (those with energies just above $\hbar\omega_c^{(\infty)}$) is opposite to that of the corresponding evaporated atoms there is an approximate compensation between the flight times in the liquid and in the vacuum for different phonon wavevectors. As a result of this compensation there is little variation in the total time of flight (equation (3)) for most phonon$\rightarrow$atom processes. The detected atom pulse shapes are therefore quite narrow, and there is little difference in the signal shapes observed at different detector positions. The variation in the amplitude of the detected phonon$\rightarrow$atom signals with angle is shown in figure 6(*a*).

To examine the dependence of the angle of evaporation on the angle of incidence at the surface, two much larger angles of incidence are used ($\theta_h = 75°$ and $\theta_h = 83°$) and the results are also shown in figure 6(*a*). Slightly higher energy input pulses of 0.2 μs at -12 dB (31.5 mW) are used for these additional measurements, but the atom pulse shapes are essentially the same as those measured with $\theta_h = 25°$. The results show clearly that an increase in the angle of incidence causes a shift in the direction

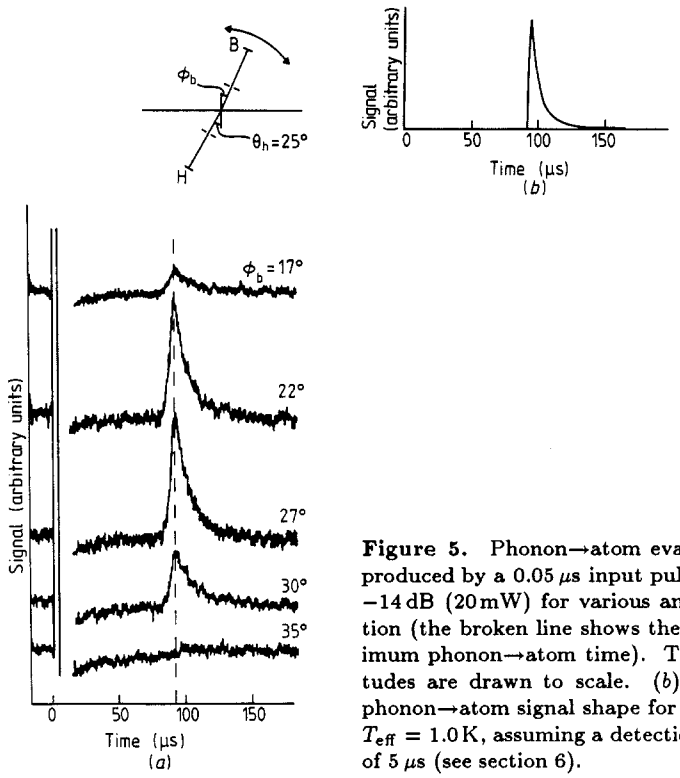

Figure 5. Phonon→atom evaporation signals produced by a 0.05 μs input pulse at a power of −14 dB (20 mW) for various angles of evaporation (the broken line shows the calculated minimum phonon→atom time). The signal amplitudes are drawn to scale. (*b*) The calculated phonon→atom signal shape for a nominal value T_{eff} = 1.0 K, assuming a detection time constant of 5 μs (see section 6).

of the evaporated atom flux to larger angles of refraction. Also, the overall refraction towards the normal expected for large angles of incidence is very clear, and the lack of any substantial difference between the θ_h = 75° and 83° distributions agrees with the behaviour anticipated for large θ from figure 2(*a*).

5.2. The evaporation of atoms by R^+ rotons

Measurements of the evaporation of atoms by injected R^+ rotons are made using a 10 μs input pulse at −24 dB (2 mW). The angular dependence of the atom signal is shown in figure 7(*a*) for the heater position θ_h = 14°. The experimental traces are drawn with similar peak heights in order to show the changes in the pulse shapes as the detector angle is varied.

The atom signals occur over a large range of evaporation angles, with the maximum flux being detected at $\phi_b \simeq 40°$ for θ_h = 14°. At small values of ϕ_b the signal is narrow and is dominated by R^+ rotons with $2.2 \lesssim q \lesssim 2.4$ Å^{-1}. At large values of ϕ_b the signal is produced by rotons from closer to the roton minimum and is therefore more dispersed in time. The minimum signal time of 71 ± 1 μs agrees well with the value of 69 μs calculated for the excitation and atom path lengths used. At the largest evaporation angles the R^+ roton→atom processes which give rise to the shortest total time are not seen by the detector. The signal detected at these angles therefore does not have a fast take-off at the calculated minimum time, as can be seen in figure 7(*a*) for ϕ_b = 75°.

The angular distribution of the detected energy for two different input powers is shown in figure 8(*a*). The powers used are −24 dB (2 mW) and −27 dB (1 mW). On

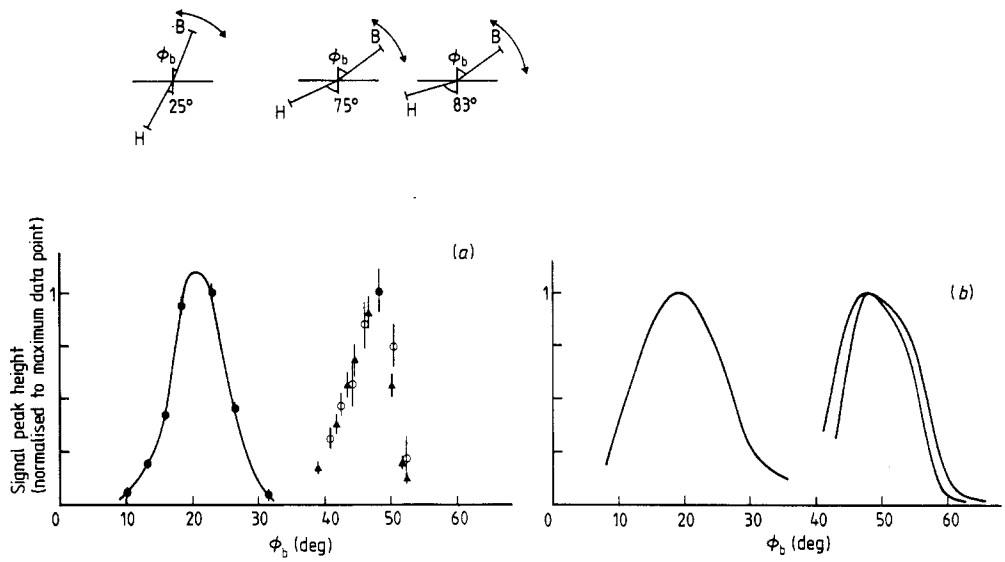

Figure 6. (*a*) The angular dependence of the peak height of the measured phonon→atom signals for three different angles of incidence. Each distribution is normalised to the maximum data point. Full circles, $\theta_h = 25°$, 0.05 μs, −14 dB; full triangles, $\theta_h = 75°$, 0.2 μs, −12 dB; open circles, $\theta_h = 83°$, 0.2 μs, −12 dB. (*b*) The calculated angular dependence obtained from the peak height of the modelled signal shapes.

the basis of the time-of-flight relation, equation (3), the integration over time up to 160 μs after the drive pulse includes evaporation by rotons with wavevectors in the range $2.0 \lesssim q \lesssim 2.6$ Å^{-1}. The graphs are normalised to the same maximum value for each power to show the changes in the angular distributions. These distributions are not strongly dependent on the input power, the only significant change being the enhancement of the signal at large values of ϕ_b for the lower input power, −27 dB. This result indicates a slight shift in the spectrum of rotons towards the roton minimum in $\omega(q)$ as the power is decreased. Such behaviour is consistent with a drop in the effective temperature describing the injected population (see section 6).

Taken together, figures 5–8 give very direct evidence for the changes in direction expected at the free surface on the basis of conservation of transverse momentum. The different features expected for phonon→atom and R^+ roton→atom evaporation are clearly observed, and in particular for the case of evaporation by phonons shown in figure 6(*a*), the dependence on the angle of incidence is very clear.

5.3. R^+ roton→atom evaporation near the critical angle

A particularly sensitive test of the details of evaporation by R^+ rotons is provided by considering the behaviour when the angles of incidence are close to the critical angles, $\theta_c(q)$ [8]. For most roton wavevectors, θ_c is between $\sim 15°$ and $\sim 25°$, as can be seen from figure 2(*a*). Measurements of this type are made by keeping the detector at a fixed angle, $\phi_b = 75°$ in our experiment, and moving the heater through the range $10° \lesssim \theta_h \lesssim 30°$.

The qualitative behaviour can be seen in figure 9. The full horizontal line at $\phi = 75°$ shows the position of the detector, and the broken horizontal lines indicate

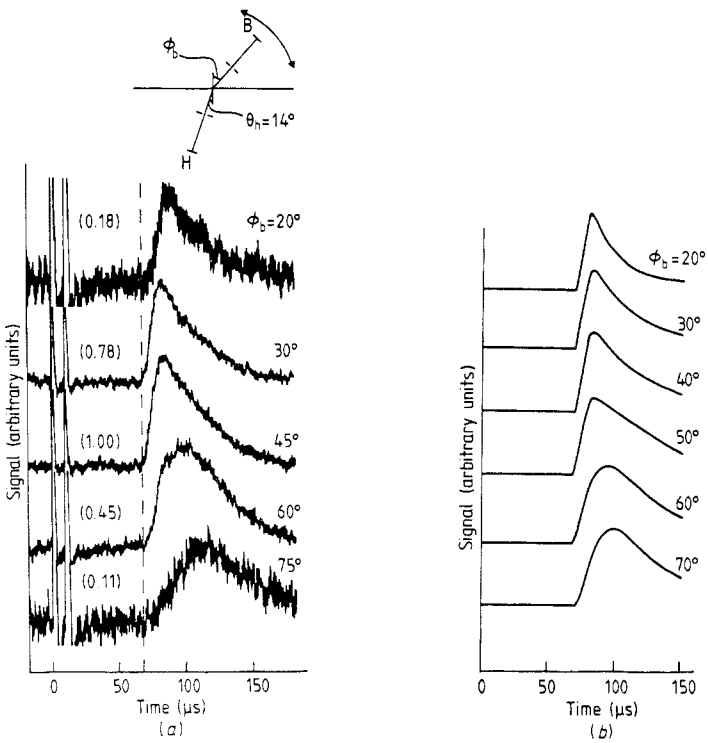

Figure 7. (*a*) R^+ roton→atom signals obtained using a 10 μs input pulse at −24 dB (2 mW) at various angles of evaporation. The relative amplitudes of the signals are shown by the numbers in brackets. The broken line shows the calculated R^+ roton→atom minimum signal time. (*b*) Modelled R^+ roton→atom pulse shapes for different evaporation angles ϕ_b, using T_{eff} = 1.5 K. The detection time constant is 5 μs.

the range of angles defined by the bolometer area and its collimator (this range is $\sim \pm 10°$ on either side of the nominal direction ϕ_b, the same as shown for the heater in figure 3). For the heater position $\theta_h = 10°$, and allowing $\pm 10°$ for the range of angles of incidence defined by the heater area and its collimator, the evaporation processes which may contribute to the atom signal are shown by the shaded area marked 'A'. The evaporation signal in this case is produced by R^+ rotons with wavevectors close to $q_{min} = 1.92\,\text{Å}^{-1}$. Increasing θ_h to 30° moves the area of interest to the shaded region marked 'B' in the diagram, which is for rotons with higher wavevectors. From the calculated total flight times as a function of excitation wavevector, the signals due to the excitations of region 'A' should produce an evaporation signal that is quite dispersed in time, whereas moving towards $\theta_h = 30°$ the signal due to the rotons from region 'B' will be significantly faster. Hence over this relatively small range of heater positions there should be a considerable change in the received signal shape.

The experimental results are shown in figure 10(*a*) for a 10 μs input pulse at a power of −24 dB (2 mW). The result at $\theta_h = 30°$ is not shown in the figure because the signal amplitude is too small to measure sensibly. An increase in the value of θ_h from 11° to 25° does indeed produce a dramatic change in the observed signal shape, with the signal being fastest with the largest angles of incidence. Figure 10(*b*) shows the results of detailed calculations of the expected signal shapes (see section 6), and these show good agreement with the measured results.

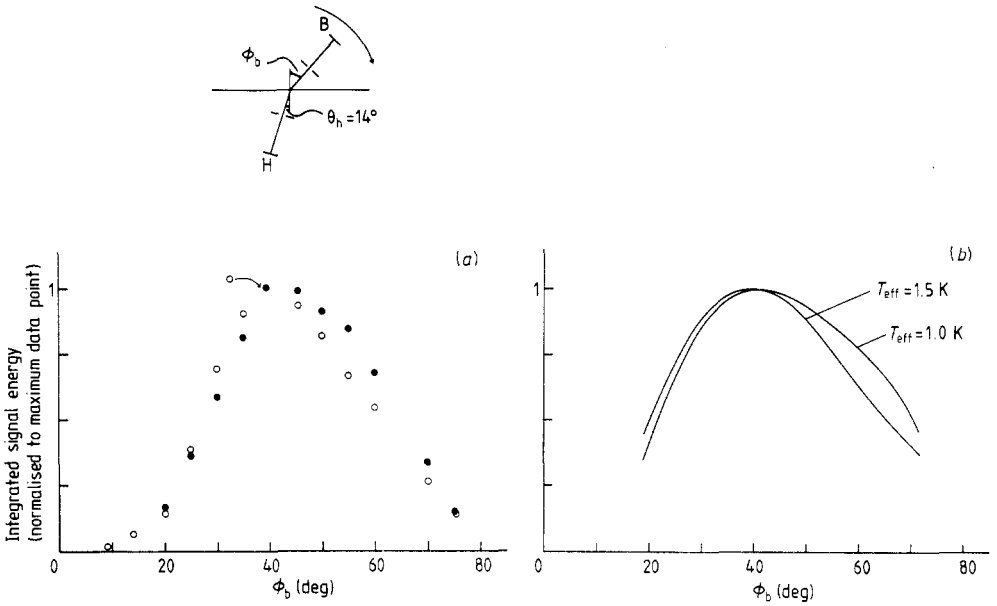

Figure 8. The angular dependence of the integrated R^+ roton→atom signal energy. The signals are integrated up to 160 μs after the start of the input pulse. Open circles, −24 dB; full circles, −27 dB. (*b*) Calculated angular distributions of the signal energy for two effective temperatures, $T_{eff} = 1.0$ K and $T_{eff} = 1.5$ K, obtained by integrating the modelled pulse shapes over the same time as the experimental measurements.

To show the angular dependence of the total atom flux the signals are integrated over time as shown in figure 11(*a*). The integration time (up to 150 μs after the start of the input pulse) is slightly shorter than that used in figure 8 because of the poor signal baselines. There is a well defined angular distribution with a maximum signal when $\theta_h \simeq 20°$, which agrees very well with the results obtained when the same integration is performed on the modelled signals (figure 11(*b*)), as discussed in section 6.

5.4. The evaporation of atoms by R^- rotons

The evaporation of atoms by R^- rotons should be identifiable either by the evaporation of atoms into a different angular quadrant (as indicated in figure 2(*b*)), or by observing a signal with the appropriate minimum arrival time, which is different from both the phonon→atom and R^+ roton→atom minimum times (figure 1(*c*)). As has been mentioned above, no processes of this type have ever been observed using this particular experimental arrangement. However, recent experiments [7] indicate that ballistic R^- rotons can be created by condensing atoms and that they have long mean-free-paths.

One explanation for the absence of a signal due to R^- rotons is that these excitations are not produced by the type of heater used. However, there is no obvious reason why there should be any difference between the ways in which R^- rotons and R^+ rotons are generated. Another possibility is that R^- rotons *are* generated by the heater but fail to reach the free surface because of interactions with other injected excitations in the bulk liquid. Such an attenuation could arise from the same sort of processes that cause the saturation of the high-energy phonon signals, as described in section 4. The maximum velocity for R^- rotons is $\simeq 150\,\mathrm{ms}^{-1}$ [25], substantially less

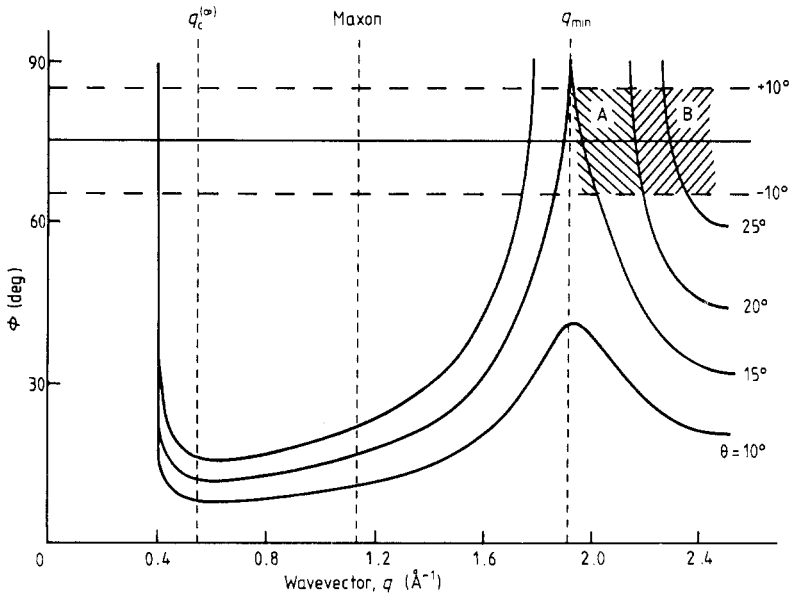

Figure 9. The evaporation of atoms by R^+ rotons into large angles ϕ. The two shaded regions indicate the excitations which can in principle contribute to the evaporation signals at $\phi_b = 75°$ for two different heater positions $\theta_h = 10°$ ('A') and $\theta_h = 30°$ ('B'). The ranges of angles of incidence and evaporation defined by the experimental collimation geometry are taken as $\pm 10°$ about the nominal positions $\theta = \theta_h$ and $\phi = \phi_b$.

than that of phonons and the fastest R^+ rotons. Any ballistic R^- rotons that are injected into the excitation beam may therefore be scattered by interactions with faster excitations generated later on in the input pulse. At very low input powers this type of scattering should cease to be effective since the injected excitation density will be very small, so in this limit it may be possible to observe R^- roton→atom evaporation with a careful choice of input conditions using this type of thin film heater.

5.5. The time of flight of phonon–atom signals

The recent neutron scattering determination of $\omega(q)$ [15], which covers the region of anomalous dispersion up to the high-energy phonon modes around $\hbar\omega \sim 12$ K, now allows detailed values for the phonon group velocities to be obtained. All the phonon→atom calculations in this paper use a polynomial fit to this data, and should give a predicted minimum flight time for the phonon→atom process, which from the quoted uncertainties in ω and q is reliable to $\sim \pm 1\,\mu$s. However, as was seen in figure 4(*a*), the measured minimum arrival time for phonon→atom signals is significantly smaller than that calculated on the basis of equation (1) for atoms evaporated by ballistic phonons. This discrepancy remains a mystery as all estimates of possible systematic errors in our experiments are not large enough to account for it. Equally, it is unlikely that there is an unidentified systematic error in the neutron data. We do not doubt the conservation of energy condition, equation (1), since the overall agree-

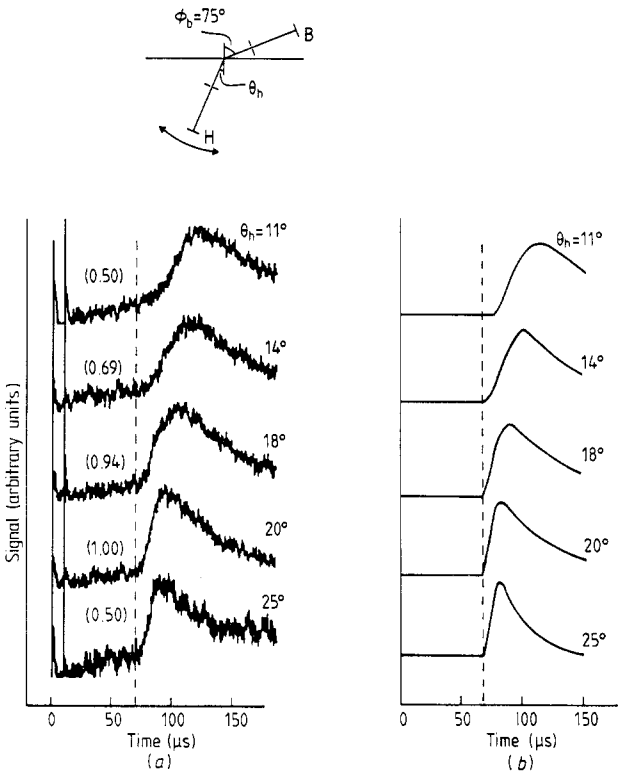

Figure 10. (*a*) The R^+ roton→atom signals at $\phi_b = 75°$ for several different heater positions θ_h, obtained using a 10 μs input pulse −24 dB (2 mW). The relative signal amplitudes are shown by the numbers in brackets. The broken line indicates the calculated R^+ roton→atom minimum signal time. (*b*) Calculated signals shapes using $T_{eff} = 1.5$ K and a detection time constant of 5 μs, to be compared with (*a*).

ment between the measured and predicted evaporation results is generally so good. The dependence of the phonon→atom signal on angle of incidence (figure 6) clearly agrees with that predicted for quantum evaporation.

6. Modelling

From the arguments given in the previous section it is clear that the measured details of the evaporation of atoms in these experiments is generally consistent with the ballistic propagation of phonons and R^+ rotons in the liquid and the subsequent quantum evaporation of atoms at the free surface. In attempting a quantitative analysis of the results two main problems arise. Firstly, because of the limited collimation many different geometrical paths have to be included. Also, there is no way of independently determining the spectrum of excitations that arrive at the liquid surface. To overcome the difficulties of doing the geometrical integrations a Monte Carlo approach is adopted, which traces individual excitation→atom trajectories through the experiment. The geometry of the heater, collimators and bolometer are then allowed for in detail. The model assumes entirely ballistic propagation in the liquid and in the vacuum, and that the evaporation of atoms is determined strictly by the conservation

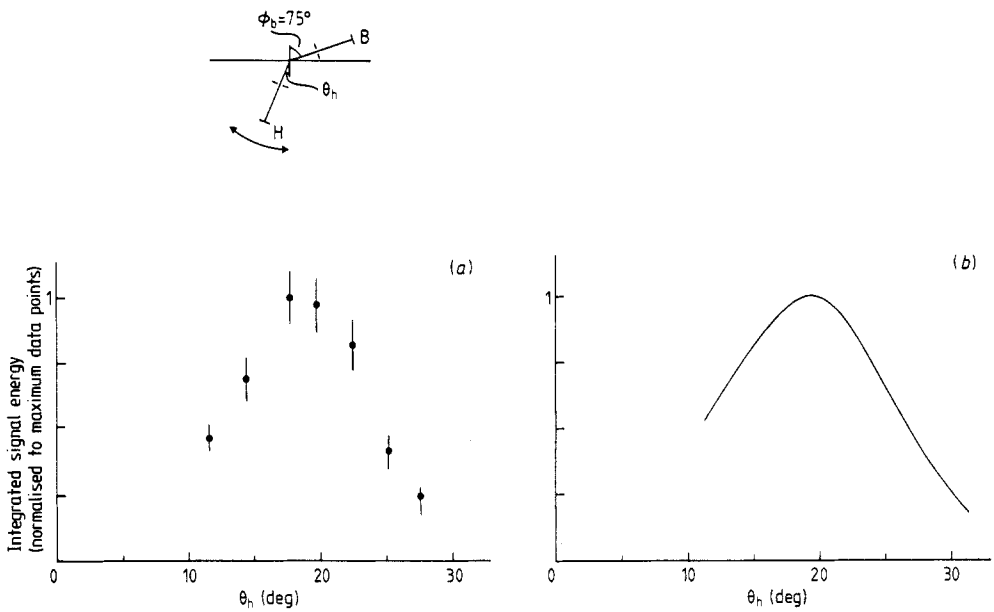

Figure 11. (*a*) The angular dependence of the R^+ roton→atom energy in the signals of figure 10(*a*), integrated up to 150 μs after the start of the input pulse. (*b*) The calculated angular dependence of the signal energy, for T_{eff} = 1.5 K, obtained by integrating the modelled signal shapes over the same time as the experimental measurements.

conditions of equations (1) and (2). The quantum efficiency for the desorption of atoms is taken to be the same for all excitations arriving at the surface at angles of incidence less than the critical angles $\theta_c(q)$. However, it is likely that there is some dependence, as yet unknown, on the wavevector and angle of incidence at the surface.

It is assumed that the energy distribution of excitations arriving at the surface can be described by the Bose–Einstein distribution function, based on the density of states in bulk liquid helium, and characterised by an effective temperature T_{eff}, i.e.

$$n(q) \propto \frac{q^2}{\exp(\hbar\omega(q)/kT_{eff}) - 1} \tag{4}$$

where $n(q)dq$ is the number of excitations in the momentum interval q to $q+dq$. Since the evaporation process at the surface requires the excitations to have a minimum energy of E_b = 7.16 K, and T_{eff} is typically 1 − 2 K, the factor $\hbar\omega/kT_{eff}$ is much greater than unity, and the spectrum is dominated by the exponential term. It is not clear whether the appropriate density of states should really reflect the dispersion of excitations in the liquid or of phonons in the heater. However, because we are using T_{eff} as a fitting parameter, the density of states function cannot be deduced independently, since to a large extent the effect of different choices of this function can be offset by using different values for the effective temperature. Values of T_{eff} are chosen to give the best agreement between the measured and modelled pulse shapes.

For a polycrystalline heater film of the type used here there is no strong angular dependence in the emission of phonons [26]. Each point on the surface of the heater is therefore assumed to emit excitations isotropically into the liquid, which is a good approximation over the small solid angle defined by the first collimator.

The atoms which reach the bolometer arrive at nearly normal incidence to the superfluid film covering its surface, and so condense with with almost 100% probability [11]. Each atom will create one, or possibly more, excitations in the superfluid film with a total energy equal to that of the original phonon or roton that caused the evaporation from the bulk. This is because the binding energy of 7.16 K is regained on condensation. We assume that the bolometer response is just proportional to the energy of these excitations created by the atom.

The thermal response time of the coupled helium film and bolometer when above the bulk liquid surface, as used in evaporation measurements, is considerably longer than that of the same bolometer when operated in the bulk liquid [21]. This can be seen in the response of the bolometer to a square light pulse produced by a visible red-light emitting diode, operated in the experiment at $\sim$ 100 mK. Measurements made with the bolometer immersed in bulk liquid helium indicate a time constant of less than 1 μs [21]. The results of similar measurements made with the bolometer above the surface show that the higher the bolometer is above the free surface, the slower the overall response. This behaviour is to be expected from the variation in the thickness of the superfluid film covering the bolometer as the height above the liquid is altered. As the superfluid film thickness is reduced, the thermal anchoring to the surroundings becomes poorer and the time taken for recovery to the ambient temperature increases. Although the response of the detector to a pulse of ^{4}He atoms may not be the same as for photons that are absorbed directly by the zinc film, the LED measurements give an indication that the bolometer response time is of the order of $\sim$ 5 μs, and this value is used here for the purpose of modelling the atom signal shapes.

7. Discussion

The modelled phonon→atom signal shapes are insensitive to the value of T_{eff} used, and show little dependence on the angles of incidence, as is found in the measured results. This is due to the fact that the velocity dispersion of phonons is roughly opposite to that of the corresponding evaporated atoms, thus giving rise to evaporation signals that are very narrow in time. Most of the width of the signals is therefore due to the time constant of the bolometer, as shown by the calculated signal shape in figure 5(*b*). The predicted angular distribution of the energy detected in the atom signals is shown in figure 6(*b*) for the same three heater positions used for the measurements. The distributions for small and large values of θ_{h} are well separated in angle, and peak close to the measured positions, which strongly reinforces the interpretation of the data given in section 5.1. In particular, it is clear that under the correct conditions (i.e. using appropriate input pulses and low ambient temperatures) the evaporation of atoms by bulk phonons is by single-excitation→single-atom processes.

A similar calculation for the evaporation of atoms by R^+ rotons gives the results of figures 7(*b*). The calculated R^+ roton→atom pulse shapes depend quite strongly on the effective temperature used to describe the spectrum. The value $T_{\text{eff}} = 1.5$ K is found to give a reasonable description of the atom signals produced by a -24 dB (2 mW) input pulse. The variation in the shapes of the atom pulses as a function of ϕ_{b} are well reproduced. Similar agreement is obtained for the results at large refraction angles, as shown by a comparison of figures 10(*a*) and 10(*b*).

The predicted angular distribution of the energy in the atom signals of figure 7(*a*) is shown in figure 8(*b*) for two effective temperatures. The overall agreement with

the measurements is very good. In particular, the effect of reducing the input power to −27 dB (1 mW), which should reduce the effective temperature of the injected roton spectrum, is supported by the calculated results. By reducing the effective temperature, the relative amplitude of the signal at large angles ϕ_b produced by low-energy R^+ rotons is increased. A similar calculation for the evaporation into large angles of evaporation is given in figure 11(*b*).

We now turn to the question of whether ripplons are associated with the evaporation process. It has been suggested that they are created in the process of a ^4He atom condensing onto the surface of liquid ^4He [27, 28] although there is no direct evidence for this. If it is possible for a phonon or roton to create an evaporated atom together with a ripplon or two then the boundary equations, equations (1) and (2), need modifying. The evaporated atom will have less energy and momentum so both its time of flight and angle of evaporation will be modified (figure 12). This will appear as a longer total signal time and a change in the angular distribution of the evaporated atoms.

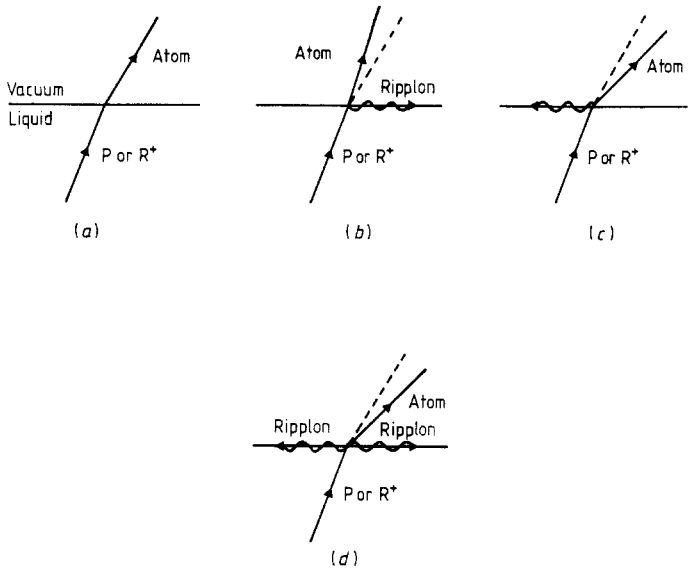

Figure 12. A schematic diagram showing the effect of ripplon emission at the surface in a quantum evaporation process. (*a*) No ripplon emission. (*b*) and (*c*) The emission of a single ripplon. (*d*) The emission of two ripplons in opposite directions.

If ripplons are created in all directions in the plane of the liquid surface then the angular distribution will be broadened. For example, ripplons with $q = 0.1\,\text{Å}^{-1}$ will increase the angular width by $\sim 10°$. The phonon→atom signals have a narrower angular width than the roton→atom ones so any broadening would be more noticeable with the former. However the angular width of the phonon evaporation is narrower than that calculated from the geometry and has a full width at half height of $\sim 10°$, so it is very unlikely that this includes a significant ripplon contribution. On this basis we put an upper limit on ripplon wavevectors of $q \sim 0.05 \pm 0.05\,\text{Å}^{-1}$.

A pair of ripplons produced with no total momentum (figure 12(*d*)) will give less broadening. For example for phonons incident at $\theta_h = 75°$, producing two ripplons, each with $q = 0.1\,\text{Å}^{-1}$, increases the angle of evaporation ϕ by $\sim 7°$. The measured

position of the maximum of the angular distribution (figure 6(*a*)) is within $\sim 3°$ of that calculated, and so from this we put an upper limit on pairs of ripplons of $q = 0.1\,\text{Å}^{-1}$ each.

The times of flight for the atom and hence the total time for phonon→atom and roton→atom processes, is changed by $3\,\mu$s if one ripplon of $q = 0.1\,\text{Å}^{-1}$ is produced. The time doubles if two ripplons are produced. We measure a phonon→atom signal that is faster than calculated so this provides no evidence for ripplon production. The minimum roton→atom time is as calculated so at least rotons with $q \sim 2.3\,\text{Å}^{-1}$ can evaporate without producing ripplons. We conclude that there is no evidence in our results that indicates ripplons are involved in the evaporation process.

Another question that can be reconsidered in the light of these latest measurements is whether or not R^+ rotons with wavevectors in the range $2.2 \lesssim q \lesssim 2.4\,\text{Å}^{-1}$ can spontaneously decay by the emission of an ultrasonic phonon i.e. the Pitaevskii process [19]. As discussed earlier, this requires the group velocity of these rotons to exceed the ultrasonic phonon velocity. If such a process does occur with a mean-free-path that is substantially less than the propagation distance of ~ 6.5 mm used here, then the contribution to the evaporation signals due to these rotons would be later or absent, depending on the scattering angle. Figure 13 shows the calculated effect (based on the model described in section 6) of removing different groups of rotons from the spectrum arriving at the surface. It can be seen that the removal of R^+ rotons in the range $2.215 \lesssim q \lesssim 2.265\,\text{Å}^{-1}$ produces a measurable change in the calculated atom signal shape. As shown in figure 13(*a*) the measured atom signals do not show any such effect. If the scattered rotons are detected we estimate that this would halve the effect on the signal shape, so we think it is reasonable to say that the maximum range for these decay processes is $2.19 \lesssim q \lesssim 2.29\,\text{Å}^{-1}$, thus confirming earlier conclusions [20]. However we are sensitive to lifetimes that are $\sim 10^5$ longer than those detectable by neutrons and so we can exclude a $\sim 10^5$ times weaker Pitaevskii process.

8. Summary and conclusions

The principal aim of the work described in this paper is to examine some of the detailed predictions of the quantum evaporation model for atom desorption from liquid helium. Previous experiments have given results that are consistent with this model for evaporation by phonons and R^+ rotons, but the present work confirms this interpretation in much more detail. Using appropriate input pulses, the results show that the parallel momentum and energy conservation conditions at the surface are well obeyed over a wide range of angles of incidence.

Well defined refraction effects are seen for both phonon→atom and R^+ roton→atom evaporation, and the angular positions and widths of the evaporated atom fluxes agree favourably with the model. The difference in behaviour observed for these two types of excitation is clearly consistent with the large difference in their total momentum. In particular, the evaporation of atoms by R^+ rotons obeys the single-excitation→single-atom conservation conditions even when the angles of incidence are close to the calculated critical angles.

These results also show that ripplon emission at the surface cannot play a very significant role in the atom desorption process, since the angular distributions of evaporated atoms would be different to that observed. The largest wavevector ripplons that could be involved without producing a measurable angular effect in the present experiment is $q \lesssim 0.1\,\text{Å}^{-1}$.

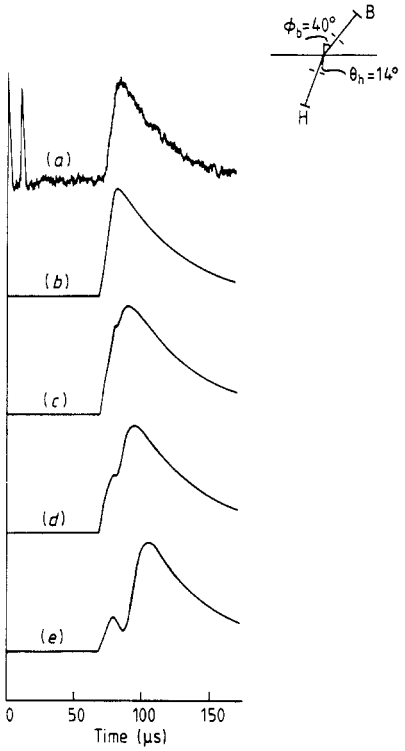

Figure 13. (*a*) The measured R^+ roton→atom signal for a 10 μs input pulse at −24 dB (2 mW). (*b*) to (e) The calculated effect on the R^+ roton→atom signal shapes of a strong spontaneous decay process which removes R^+ rotons within a range of wavevectors Δq. The value $T_{\text{eff}} = 1.5$ K is used for the calculation, and a detection time constant of 5 μs is assumed. (*b*), $\Delta q = 0$; (*c*) $2.215 < q < 2.265 \text{Å}^{-1}$, removed ($\Delta q = 0.05 \text{Å}^{-1}$); (*d*) $2.19 < q < 2.29 \text{Å}^{-1}$, removed ($\Delta q = 0.1 \text{Å}^{-1}$); (*e*) $2.14 < q < 2.34 \text{Å}^{-1}$, removed ($\Delta q = 0.2 \text{Å}^{-1}$).

The good qualitative agreement between the measured R^+ roton→atom pulse shapes and those calculated on the basis of ballistic propagation in the liquid confirms that at low temperatures the majority of R^+ rotons do have macroscopic mean-free-paths of at least several millimetres. Also, from a comparison between the measured and calculated atom signal shapes it can be concluded that any strong spontaneous decay process for those R^+ rotons with the largest group velocities is limited to a narrow range of wavevectors just below $q \sim 2.3 \text{ Å}^{-1}$.

Apart from developing our understanding of the microscopic processes at the free surface, our knowledge about this system for R^+ rotons opens up the possibility of some roton spectroscopy. This has not been possible in the past because ballistic rotons are so difficult to detect in the bulk liquid. The evaporation process at the surface not only makes the energy of the roton detectable, but the wavevector dependence of the combined flight time of the excitation and atom also provides some spectroscopic resolution.

Acknowledgments

We would like to acknowledge the skilled technical assistance of Melvin Gear at all

stages of the experimental work for this project. This work was supported by the SERC, and one of us (MB) is grateful to the SERC for a research studentship.

References

[1] Baird M J, Hope F R and Wyatt A F G 1983 *Nature* **304** 325
[2] Hope F R, Baird M J and Wyatt A F G 1984 *Phys. Rev. Lett.* **52** 1528
[3] Wyatt A F G 1983 *Proc. 75th Jubilee Conf. on* ^{4}*He* ed J G M Armitage (Singapore: World Scientific) p117
[4] Osborne D V 1962 *Proc. Phys. Soc.* **80** 1343
[5] Anderson P W 1972 *Phys. Lett.* **29A** 563
[6] Cole M W 1972 *Phys. Rev. Lett.* **28** 1622
[7] Wyborn G M and Wyatt A F G 1990 to be published
[8] Wyatt A F G 1984 *Physica* B **126** 392
[9] Balibar S, Buechner J, Castaing B, Laroche C and Libchaber A 1978 *Phys. Rev.* B **18** 3096
[10] Hyman D S, Scully M O and Widom A 1969 *Phys. Rev.* **186** 231
[11] Nayak V U, Edwards D O and Masuhara N 1983 *Phys. Rev. Lett.* **50** 990
[12] Fozooni P, Spencer D S and Lea M J 1987 *Japan. J. Appl. Phys.* **26-3** 281
[13] van Dijk H, Durieux M, Clement J R and Logan J K 1960 *J. Res. NBS* A **64** 1
[14] Maris H J and Massey W E 1970 *Phys. Rev. Lett.* **25** 220
[15] Stirling W G 1983 *Proc. 75th Jubilee Conf. on* ^{4}*He* ed J G M Armitage (Singapore: World Scientific) p109, and private communication
[16] Sluckin T J and Bowley R M 1974 *J. Phys. C: Solid State Phys.* **7** 1779
[17] Maris H J 1977 *Rev. Mod. Phys.* **49** 341
[18] Dynes R C and Narayanamurti V 1975 *Phys. Rev.* B **12** 1720
[19] Pitaevskii L P 1959 *Sov. Phys.-JETP* **36(9)** 830
[20] Mezei F 1980 *Phys. Rev. Lett.* **44** 1601
[21] Wyatt A F G, Sherlock R A and Allum D R 1982 *J. Phys. C: Solid State Phys.* **15** 1897
[22] Brown M and Wyatt A F G 1990 to be published
[23] Baird M J, Richards B and Wyatt A F G 1987 *Japan. J. Appl. Phys.* **26-3** 387
[24] Brown M and Wyatt A F G 1987 *Japan. J. Appl. Phys.* **26-3** 385
[25] Cowley R A and Woods A D B 1971 *Can. J. Phys.* **49** 177
[26] Mills N G, Wyatt A F G and Sherlock R A 1975 *J. Phys. C: Solid State Phys.* **8** 289
[27] Echenique P M and Pendry J B 1976 *Phys. Rev. Lett.* **37** 561
[28] Edwards D O, Ihas G G and Tam C P 1977 *Phys. Rev.* B **16** 3122